A High-Order Compact Finite Difference Decoupling Approach for Reissner-Mindlin Plate Bending

Horria S. El Gendy
Basic Engineering Sciences Department, Benha Faculty of Engineering, Benha University, Benha 13512, Egypt
horria.elgendy@bhit.bu.edu.eg

Mourad S. Semary
Basic Engineering Sciences Department, Benha Faculty of Engineering, Benha University, Benha 13512, Egypt | Faculty of Engineering, Badr University in Cairo BUC, Cairo 11829, Egypt
mourad.semary@yahoo.com

Tamer M. Rageh
Basic Engineering Sciences Department, Benha Faculty of Engineering, Benha University, Benha 13512, Egypt
tamer.rageh@bhit.bu.edu.eg

Kamal Hassan
Department of Basic Science, Informatic and Computer Science, The British University in Egypt, Cairo, Egypt
kamal.hassan@bue.edu.eg (corresponding author)

Received: 29 April 2025 | Revised: 24 May 2025 and 14 June 2025 | Accepted: 3 July 2025

 DOI: https://doi.org/10.48084/etasr.11821

ABSTRACT

This study presents a novel and computationally efficient framework for solving high-order Partial Differential Equations (PDEs), particularly polyharmonic equations, by systematically decomposing them into a sequence of coupled second-order problems. The core contribution lies in enhancing the classical decoupling strategies by introducing a Compact Finite Difference (CFD) scheme with improved numerical stability, accuracy, and flexibility. This method was previously applied to fourth-order differential equations in an earlier study. The current study extends the application of this method to sixth-order PDEs, particularly those arising in plate bending problems governed by the Reissner–Mindlin (R-M) theory. Specifically, a modified single-variable formulation proposed by the Bergan-Wang model was considered the study. The novelty of this approach lies in the streamlined reduction of polyharmonic operators using consistent Poisson-like solvers; a convergence-enhanced compact discretization applicable to various boundary conditions; and numerical benchmarking against recent Finite Element Methods (FEMs). Extensive simulations demonstrate the method's capability in computing accurate displacement and stress fields over different geometries and boundary types, suggesting its viability for complex engineering applications.

Keywords-triharmonic PDEs; decoupling-coupling methods; plate bending; Reissner–Mindlin theory; finite difference; compact finite difference schemes

I. INTRODUCTION

The polyharmonic equation, a higher-order PDE, plays an important role in various branches of applied mathematics and engineering, particularly in the fields of elasticity theory, fluid mechanics, and plate bending problems. This equation arises naturally when modeling physical phenomena that involve the bending of elastic plates or the flow of viscous fluids. Given its wide range of applications, the accurate and efficient solution of the polyharmonic equation is of great interest in both theoretical and computational studies. In many practical scenarios, the polyharmonic equation is subjected to boundary

conditions that significantly influence the behavior of its solutions.

Various numerical solution techniques have been examined in the literature for both 2D biharmonic and tri-harmonic equations. This includes the investigation of three meshless methods for solving boundary value problems: the special-purpose Trefftz function method, the method of fundamental solutions, and the symmetric method of fundamental solutions. These methods have been compared for harmonic and biharmonic equations, with particular attention to their convergence properties and error-reduction capabilities [1]. Another study presented an improved FEM to account for increased stability and accuracy under different sets of boundary conditions. Authors in [2], introduced differencing methods of $O(h^4)$ accuracy to solve the two-dimensional multi-harmonic elliptic equations on the squiggly mesh, using the nine-point single cell. High-order accuracy methods for multi-dimensional biharmonic equations of the second kind were discussed in [3]. As with the staggered configuration, a fourth-order discretization was developed in [4] to solve two-dimensional elliptic equations on an unequal mesh. Authors in [5] combined triharmonic and biharmonic equations to solve highly challenging problems found in real-world engineering applications. Authors in [6] studied the application of the triharmonic equation to geometric design and optimization.

In [7], the proposed method was validated through its application to a class of fourth-order differential equations with known analytical solutions. The numerical results confirmed the method's high efficiency and accuracy in resolving these problems. The current study utilizes a decoupling-coupling framework to improve the solution of polyharmonic plate bending problems. First, by employing a consistent operator decomposition strategy, the method offers a single mathematical formulation that simultaneously addresses both biharmonic and triharmonic models. Second, in contrast to conventional schemes, it uses a high-order CFD discretization, greatly improving the numerical accuracy and convergence behavior. Third, a thorough numerical validation of the framework is conducted against contemporary benchmark approaches, such as FEM. Quantitative comparisons are made regarding the convergence rates and displacement accuracy. This method, which is practical and flexible for real-world applications, involving complex high-order PDEs, works well with a variety of boundary conditions and geometries when implemented in MATLAB. The primary implementation focuses on uniform Cartesian grids for clarity and benchmarking; however, the formulation is inherently extendable to irregular domains and non-uniform meshes, laying the foundation for future generalizations.

II. POLYHARMONIC EQUATION

A. Biharmonic Equations

For biharmonic problems, which involve fourth-order PDEs, two categories of numerical approaches are widely applied. The first one is called a direct or uncoupled approach, which considers approximating the fourth order differential operator, found in [8-10]. The direct approach along with the finite difference discretization also fall broadly into two categories. Authors in [8] directly approximate the biharmonic operator with second-order accuracy but they use 13-points in 2D and 27- points in 3D, which destroy the compactness of the finite difference method, requiring extra treatments near the boundary.

The results and methodologies of this study can be extended to more complex and general systems of equations, such as $w(x, y)$ [11]:

$$\Delta^2 w = f(x,y)\ in\ \Omega,\quad w = 0\ and\ \frac{\partial w}{\partial n} = 0\ on\ \Gamma \quad (1)$$

where $\Omega = (0.1)\times(0.1)$ with specified boundary conditions. The notation $\partial w/\partial n$ refers to the normal derivative on the boundary of the unit square, where n is a unit vector orthogonal to the surface:

$$\frac{\partial \mathrm{w}}{\partial \mathrm{n}} = \begin{cases} \frac{\partial \mathrm{w}}{\partial \mathrm{x}} = 0, & 0 \le y \le 1 \\ \frac{\partial \mathrm{w}}{\partial \mathrm{y}} = 0, & 0 \le x \le 1 \end{cases} \quad (2)$$

recalling:

$$\Delta^2 w = \frac{\partial^4 w}{\partial \mathrm{x}^4} + 2\frac{\partial^4 w}{\partial \mathrm{x}^2 \partial y^2} + \frac{\partial^4 w}{\partial y^4} = f(x,y) \quad (3)$$

This novel method simplifies the fourth-order problem by breaking it down into two second-order problems, facilitating a more straightforward implementation. Equation (1) can be replaced by:

$$\Delta w \equiv w^{xx} + w^{yy} = v, \quad (4)$$
$$\Delta v \equiv v^{xx} + v^{yy} = f(x,y)$$

where w^{xx} and w^{yy} are defined as the approximation of the second-order partial derivatives. Considering the given boundary conditions (2), the proposed approach involves solving the finite difference analog of the coupled system represented by (4) and (2).

Superimpose a square grid over the unit square with size $h = \frac{1}{N} + 1$ where N is a positive integer, Ω_h is taken as a gride point $(x, y) = (ih, jh)$ for $1 \le i, j \le N$ (i.e., the interior points), Γ_h is a boundary point, and w is a function where, $w(x, y) \equiv w_{ij}$.

A standard explicit finite difference scheme approximates the Poisson equation, utilizing a centered scheme as defined in (5). The local truncation error of this approximation is of the order $O(h^2)$ [12].

$$\Delta w = \frac{w_{i+1,j} + w_{i-1,j} + w_{i,j+1} + w_{i,j-1} - 4w_{i,j}}{h^2} \quad (5)$$

The decoupling method is implemented, and finite-difference techniques are utilized to derive the matrix representation of the coupled system presented in (4):

$$A\underline{W} = \underline{V} \quad (6)$$
$$A\underline{V} = \underline{F}$$

Combining the two expressions from (6), results in a unified global matrix equation:

$$A\left(A\underline{W}\right) = A^2\underline{W} = \underline{F} \quad (7)$$

B. Triharmonic Equations

The triharmonic problems were difficult to solve using the central difference technique, which led to the adoption of an alternative method, FEM [13]. This section focuses on solving high-order PDEs using decoupling and coupling approaches. This innovative solution simplifies the sixth-order problem by dividing it into three Poisson equations, allowing for easier implementation.

By applying the same previously introduced idea to the following triharmonic equations, for *w (x,y)* [14]:

$$\Delta^3 w = f(x,y) \quad in\ \Omega, \tag{8}$$

$$w|_\Gamma = 0, \quad \left.\frac{\partial w}{\partial n}\right|_\Gamma = 0, \quad \left.\frac{\partial^2 w}{\partial n^2}\right|_\Gamma = 0,$$

where:

$$\frac{\partial w}{\partial n} = \begin{cases} \frac{\partial w}{\partial x} = 0, & 0 \le y \le 1 \\ \frac{\partial w}{\partial y} = 0, & 0 \le x \le 1 \end{cases} \tag{9}$$

$$\frac{\partial^2 w}{\partial n^2} = \begin{cases} \frac{\partial^2 w}{\partial^2 x} = 0, & 0 \le y \le 1 \\ \frac{\partial^2 w}{\partial^2 y} = 0, & 0 \le x \le 1 \end{cases}$$

recalling:

$$\Delta^3 w = \frac{\partial^6 w}{\partial x^6} + 3\frac{\partial^6 w}{\partial x^2 \partial y^4} + 3\frac{\partial^6 w}{\partial x^4 \partial y^2} + \frac{\partial^6 w}{\partial y^6} \tag{10}$$

Now, (8) can be replaced by,

$$\Delta w \equiv w^{xx} + w^{yy} = v(x,y),$$
$$\Delta v \equiv v^{xx} + v^{yy} = u(x,y) \tag{11}$$
$$\Delta u \equiv u^{xx} + u^{yy} = f(x,y)$$

These equations can be reformulated using the proposed decoupling–coupling technique:

$$\mathrm{A}\underline{W} = \underline{V}$$
$$\mathrm{A}\underline{V} = \underline{U} \tag{12}$$
$$\mathrm{A}\underline{U} = \underline{F}$$

$$\mathrm{A}\left(\mathrm{A}\underline{W}\right) = \mathrm{A}\left(\mathrm{A}(\mathrm{A}\underline{W})\right) = \mathrm{A}^3\underline{W} = \underline{F} \tag{13}$$

where, the Matrix A for accuracy $O(h^2)$ is:

$$A = \frac{1}{h^2}\begin{pmatrix} -4 & 1 & 0 & 1 & 0 & 0 & 0 & 0 & 0 \\ 1 & -4 & 1 & 0 & 1 & 0 & 0 & 0 & 0 \\ 0 & 1 & -4 & 0 & 0 & 1 & 0 & 0 & 0 \\ 1 & 0 & 0 & -4 & 1 & 0 & 1 & 0 & 0 \\ 0 & 1 & 0 & 1 & -4 & 1 & 0 & 1 & 0 \\ 0 & 0 & 1 & 0 & 1 & -4 & 0 & 0 & 1 \\ 0 & 0 & 0 & 1 & 0 & 0 & -4 & 1 & 0 \\ 0 & 0 & 0 & 0 & 1 & 0 & 1 & -4 & 1 \\ 0 & 0 & 0 & 0 & 0 & 1 & 0 & 1 & -4 \end{pmatrix}$$

To enhance the solution accuracy to fourth-order $O(h^4)$, the traditional approach becomes increasingly complex where the fourth-order central finite differences were used to discretize second-order partial derivatives in nine points as [15]:

$$w^{xx} = \frac{-w_{i+2}+16w_{i+1}-30w_i+w_{i-1}-w_{i-2}}{12h^2}$$

$$w^{yy} = \frac{-w_{j+2}+16w_{j+1}-30w_j+w_{j-1}-w_{j-2}}{12k^2}$$

Therefore, CFD schemes, which offer the advantage of achieving higher-order accuracy with fewer cell points are used. These implicit methods, however, often involve matrix inversion when applied to solving PDEs. To optimize the computational efficiency, the matrix inversion is performed once during the initialization phase, and the inverse or the factorized form is stored. This stored matrix is then reused in subsequent iterations or time steps, significantly reducing the computational cost and improving the performance.

Specifically, second derivative CFD schemes are employed for achieving fourth-order accuracy [16]:

$$\frac{1}{10}w''_{i-1} + w''_i + \frac{1}{10}w''_{i+1} = \frac{6}{5}\frac{w_{i+1}-2w_i+w_{i-1}}{h^2}$$

The proof for the second derivative CFD formula can be found in [17]. Additionally, a rapid implementation of a fourth-order CFD scheme for the Poisson equation in two dimensions is presented as:

$$w^{xx}_{i+1,j} + 10w^{xx}_{i,j} + w^{xx}_{i-1,j} = \frac{12}{h_x^2}(w_{i+1,j} - 2w_{i,j} + w_{i-1,j})$$

$$w^{yy}_{i,j+1} + 10w^{yy}_{i,j} + w^{yy}_{i,j-1} = \frac{12}{h_y^2}(w_{i,j+1} - 2w_{i,j} + w_{i,j-1})$$

Utilizing the Kronecker product (or tensor product, ⊗), can reformulate the above equations into the following matrix form:

$$A_x \otimes I\ W^{xx} = \frac{12}{h_x^2} B_x \otimes I\ W$$

$$A_1\ W^{xx} = \frac{12}{h_x^2} B_1\, W$$

$$W^{xx} = \frac{12}{h_x^2}\, A_1^{-1}\, B_1\, W$$

$$A_y \otimes I\ W^{yy} = \frac{12}{h_y^2} B_y \otimes I\ W$$

$$A_2\ W^{yy} = \frac{12}{h_y^2} B_2\, W$$

$$W^{yy} = \frac{12}{h_y^2}\, A_2^{-1}\, B_2\, W$$

where A_x, A_y , B_x, and B_y are taken in general forms as:

$$A_x = \begin{pmatrix} 10 & 1 & 0 & \cdots & 0 & 0 \\ 1 & 10 & 1 & \cdots & 0 & 0 \\ 0 & 1 & 10 & \cdots & 0 & 0 \\ \vdots & \vdots & \vdots & \ddots & \vdots & \vdots \\ 0 & 0 & 0 & \cdots & 10 & 1 \\ 0 & 0 & 0 & \cdots & 1 & 10 \end{pmatrix},$$

$$B_x = \begin{pmatrix} -2 & 1 & 0 & \cdots & 0 & 0 \\ 1 & -2 & 1 & \cdots & 0 & 0 \\ 0 & 1 & -2 & \cdots & 0 & 0 \\ \vdots & \vdots & \vdots & \ddots & \vdots & \vdots \\ 0 & 0 & 0 & \cdots & -2 & 1 \\ 0 & 0 & 0 & \cdots & 1 & -2 \end{pmatrix}$$

$\because\ \Delta w = W^{xx} + W^{yy} = F$

$$\left(\frac{12}{h_x^2}\, A_1^{-1}\, B_1 + \frac{12}{h_y^2}\, A_2^{-1}\, B_2\right) \underline{W} = \underline{F}$$

If $h_x = h_y = h$,

$$\frac{12}{h^2}\,(A_1^{-1}\, B_1 + \, A_2^{-1}\, B_2)\, \underline{W} = \underline{F}$$

$$\underline{AW} = \underline{F}$$

where:

$$A_c = \frac{12}{h^2}\,(A_1^{-1}\, B_1 + \, A_2^{-1}\, B_2)$$

where Matrix A_c for fourth-order CFD $O(h^4)$ is:

$$A_c = \begin{pmatrix} -0.4492 & 0.1237 & -0.0125 & .. & .. & .. & 0 \\ 0.1237 & -0.4492 & 0.1237 & .. & .. & : & : \\ -0.0125 & 0.1237 & -0.4492 & .. & .. & : & : \\ : & : & : & .. & : & : & : \\ : & : & : & .. & : & : & : \\ : & : & : & .. & -0.4492 & 0.1237 & -0.0125 \\ : & .. & .. & .. & 0.1237 & -0.4492 & 0.1237 \\ 0 & .. & .. & .. & -0.0125 & 0.1237 & -0.4492 \end{pmatrix}$$

Subsequently, it is necessary to apply the boundary conditions to the matrix A^2 for the biharmonic equation or A^3 for the triharmonic equation based on the appropriate accuracy level of the matrix. This has been discussed in detail in our previous work [7].

The entire numerical procedure can be summarized as:

- Given *i, j, M, N* , and grid points $(x_i, y_j), i = 0,1, \dots, M, j = 0,1, \dots, N,$ can be computed $\underline{F}$ by the evaluation of $f(x_i, y_j)\ h$.
- Compute *A*, A^2, defined in (7), and A^3 defined in (13).
- Apply the boundary conditions on A^2 and A^3.
- Perform the matrix inversion of, A^2, A^3 and get *W*.

III. GENERAL BEHAVIOR OF SINGLE-VARIABLE VERSION OF REISSNER–MINDLIN PLATE THEORY

While Kirchhoff's plate theory provides accurate enough results for thin plate bending problems, its accuracy decreases as the plate's thickness increases. Such an intrinsic weakness of the classical plate theory [18] entailed the implementation of other, more refined hypotheses to provide accurate results for the behavior of thin and moderately thick plates [19].

To incorporate the transverse shear deformations during the analysis of the behavior of both thin and moderately thick plates, two main theories have been proposed, the first in [20], which depended on the stresses and the second in [21], which depended on the displacements as the primary variables.

Instances can be found in literature, where these two theories have been referred together as one theory known as the R-M plate theory [22]. The Bergan-Wang approach has shown that the R-M plate theory can be effectively formulated solely in terms of the transverse deflection *w (x, y),* by using an additional assumption [13, 23]. For example, rectangular finite element models utilizing this one-variable formulation demonstrate high accuracy and efficiency for both thin and thick plates [13]. Additionally, methods, such as the Virtual Element Method (VEM) [24], and the Tangential-Displacement Normal-Normal-Stress (TDNNS) method [25], also confirm the advantages of single-variable formulations in improving the accuracy and computational efficiency while eliminating the shear locking.

Authors in [20] began the formulation of a differential equations system for the analysis of the bending problem of thin and moderately thick plates, with the first assumption of linear variation over the thickness of the plate for the bending and twisting stresses:

$$\sigma_x = \frac{12 M_x Z}{h^3} \tag{14}$$

$$\sigma_y = \frac{12 M_y Z}{h^3} \tag{15}$$

$$\tau_{xy} = \frac{12 M_{xy} Z}{h^3} \tag{16}$$

By substituting these relations of the bending stresses into the set of differential equations that satisfy the equilibrium for an infinitesimal plate element [20], the expressions of the transverse shear stress components τ_{xz} and τ_{yz} and the normal stress component σ_z can be written as:

$$\tau_{xz} = \int_{-h/2}^{h/2} \frac{\partial \sigma_x}{\partial x} + \frac{\partial \tau_{xy}}{\partial y}\, dz = \frac{3Q_x}{2h}\left[1 - \left(\frac{4Z^2}{h^2}\right)\right] \tag{17}$$

$$\tau_{yz} = \int_{-h/2}^{h/2} \frac{\partial \tau_{yx}}{\partial x} + \frac{\partial \sigma_y}{\partial y}\, dz = \frac{3Q_y}{2h}\left[1 - \left(\frac{4Z^2}{h^2}\right)\right] \tag{18}$$

$$\sigma_z = \int_{-\frac{h}{2}}^{\frac{h}{2}} \frac{\partial \tau_{zx}}{\partial x} + \frac{\partial \tau_{zy}}{\partial y}\, dz = -\frac{3}{4}\left(\frac{\partial Q_x}{\partial x} + \frac{\partial Q_y}{\partial x}\right)\left[\left(\frac{2Z}{h}\right) - \left(\frac{8Z^3}{3h^3}\right)\right] \tag{19}$$

By using the equilibrium conditions on the infinitesimal rectangular plate element:

$$Q_x = -\frac{\partial M_{xy}}{\partial y} + \frac{\partial M_x}{\partial x} = -D\left[\frac{\partial^3 w}{\partial x^3} + \frac{\partial^3 w}{\partial x \partial y^2}\right] \tag{20}$$

$$Q_y = \frac{\partial M_{xy}}{\partial x} - \frac{\partial M_y}{\partial y} = -D\left[\frac{\partial^3 w}{\partial y^3} + \frac{\partial^3 w}{\partial x^2 \partial y}\right] \tag{21}$$

$$\frac{\partial Q_x}{\partial x} + \frac{\partial Q_y}{\partial y} = -P \tag{22}$$

where *D* represents the bending stiffness of the plate or the flexural rigidity of the plate and is given by: $D = \frac{Eh^3}{12(1-\nu^2)}$

Then, Reissner derived the mathematical expressions for the bending moments M_x, M_y, and the twisting moment M_{xy} by removing the variation of the strain energy Π for the homogenous plate from an isotropic material:

$$\Pi = \frac{1}{2E}\iiint\left[{\sigma_x}^2 + {\sigma_y}^2 + {\sigma_z}^2 - 2\nu\left(\sigma_x\sigma_y + \sigma_x\sigma_z + \sigma_y\sigma_z\right) + 2(1+\nu)\left({\tau_{xy}}^2 + {\tau_{xz}}^2 + {\tau_{yz}}^2\right)\right] dx\, dy\, dz = 0 \tag{23}$$

By substituting the expressions of the bending and shear stresses from (14)-(19) into (23), and first integrating concerning f *z* rom limit *-h/2* to *+h/2* and then integrate by parts and rearrange the resulting equations, this leads to the following mathematical expressions for M_x, M_y, and M_{xy}:

$$M_x = -D\left[\frac{\partial^2 w}{\partial x^2} + \nu\frac{\partial^2 w}{\partial y^2}\right] + \frac{h^2}{5(1-\nu)}\left[\frac{\partial Q_x}{\partial x} + \nu\frac{\partial Q_y}{\partial y}\right] + \frac{h^2\nu}{10(1-\nu)}q \quad (24)$$

$$M_y = -D\left[\frac{\partial^2 w}{\partial y^2} + \nu\frac{\partial^2 w}{\partial x^2}\right] + \frac{h^2}{5(1-\nu)}\left[\frac{\partial Q_y}{\partial y} + \nu\frac{\partial Q_x}{\partial x}\right] + \frac{h^2\nu}{10(1-\nu)}q \quad (25)$$

$$M_{xy} = -(1-\nu)D\left[\frac{\partial^2 w}{\partial x\partial y}\right] + \frac{h^2}{10}\left[\frac{\partial Qx}{\partial y} + \frac{\partial Qy}{\partial x}\right] \quad (26)$$

Reissner relied on his theory on the second assumption that the normal straight line to the undeformed mid-plane of the plate before bending will remain straight but not normal to the undeformed mid-plane of the plate after bending. φ_x^R inclines this straight axis about the *x*-axis and by φ_y^R about the *y*-axis, which can be expressed according to Reissner's hypothesis as:

$$\varphi_x^R = \left(-\frac{\partial w}{\partial x}\right) + \left(\frac{12(1+\nu)}{5Eh}Q_x\right) \quad (27a)$$

$$\varphi_y^R = \left(-\frac{\partial w}{\partial y}\right) + \left(\frac{12(1+\nu)}{5Eh}Q_y\right) \quad (27b)$$

$$\frac{\partial\varphi_x^R}{\partial x} + \nu\frac{\partial\varphi_y^R}{\partial y} = -\left(\frac{\partial^2 w}{\partial x^2} + \nu\frac{\partial^2 w}{\partial y^2}\right) + \frac{12(1+\nu)}{5Eh}\left(\frac{\partial Q_x}{\partial x} + \nu\frac{\partial Q_y}{\partial y}\right) \quad (28)$$

Therefore, the previous expressions of the bending and twisting moments (24-26) can be formulated again in terms of the rotation displacements φ_x^R and φ_y^R as:

$$M_x = D\left[\frac{\partial\varphi_x^R}{\partial x} + \nu\frac{\partial\varphi_y^R}{\partial y}\right] + \frac{h^2\nu}{10(1-\nu)}q \quad (29)$$

$$M_y = D\left[\frac{\partial\varphi_y^R}{\partial y} + \nu\frac{\partial\varphi_x^R}{\partial x}\right] + \frac{h^2\nu}{10(1-\nu)}q \quad (30)$$

$$M_{xy} = \frac{D(1-\nu)}{2}\left[\frac{\partial\varphi_x^R}{\partial y} + \frac{\partial\varphi_y^R}{\partial x}\right] \quad (31)$$

To create a system of differential governing equations for plate bending problems, taking into account the effect of the transverse shear, Reissner started by applying the static equilibrium conditions shown in (20-22), for an infinitesimal rectangular plate element of dimensions ($dx \times dy$) and thickness *h*, as shown in Figure 1, between the bending moments M_x, M_y, and the twisting moment M_{xy}, transverse shear resultants Q_x, Q_y, and the plane load $q(x,y)$ per unit of element area.

By substituting (24-26) into these static equilibrium equations, this stress-based hypothesis results in a system of three differential governing equations of six orders [26], which can be formulated as:

$$\Delta\Delta w = \frac{q(x,y)}{D} - \frac{h^2}{10D}\frac{2-\nu}{1-\nu}\Delta\left[\frac{\partial Q_x}{\partial x} + \frac{\partial Q_y}{\partial y}\right] \quad (32)$$

$$Q_x - \frac{h^2}{10}\Delta Q_x = -D\left[\frac{\partial^3 w}{\partial x^3} + \frac{\partial^3 w}{\partial x\partial y^2}\right] - \frac{h^2}{10(1-\nu)}\frac{\partial q(x,y)}{\partial x} \quad (33)$$

$$Q_y - \frac{h^2}{10}\Delta Q_y = -D\left[\frac{\partial^3 w}{\partial y^3} + \frac{\partial^3 w}{\partial y\partial x^2}\right] - \frac{h^2}{10(1-\nu)}\frac{\partial q(x,y)}{\partial y} \quad (34)$$

Bergan-Wang hypothesis [23, 27], which represents a modified version of the R-M theory has relied on substituting the compatibility equilibrium equation of the plate, as shown in (20) and (21), into the mathematical expressions of shear strain γ_{xz} and γ_{yz}, which gives:

$$\gamma_{xz} = \frac{1}{Ghk_s}Q_x = \frac{1}{Ghk_s}\left(-\frac{\partial M_{xy}}{\partial y} - \frac{\partial M_x}{\partial x}\right) \quad (35)$$

$$\gamma_{yz} = \frac{1}{Ghk_s}Q_y = \frac{1}{Ghk_s}\left(-\frac{\partial M_{xy}}{\partial x} - \frac{\partial M_y}{\partial y}\right) \quad (36)$$

where *G* is the shear modulus and *h* is the thickness of the plate. By taking the shear correction factor k_s = 5/6, according to Mindlin hypothesis, and using the mathematical expressions of the bending moments M_x, M_y, and the twisting moment M_{xy}, according to the Mindlin plate theory, as shown in (29-31), considering the definitions of the rotations of the normal axis on the middle plane of the plate after the deformation, the resulting φ_x^R and φ_y^R are as shown in into the above equations of γ_{xz} and γ_{yz}, which can be expressed as [13]:

$$\varphi_x^R = \frac{\partial w}{\partial x} - \gamma_{xz} \quad (37)$$

$$\varphi_y^R = \frac{\partial w}{\partial y} - \gamma_{yz} \quad (38)$$

$$\gamma_{xz} = \frac{h^2}{5(1-\nu)}\left[\frac{\partial^3 w}{\partial x^3} + \frac{\partial^3 w}{\partial x\partial y^2} + \frac{\partial^2\gamma_{xz}}{\partial x^2} + \frac{(1-\nu)}{2}\frac{\partial^2\gamma_{xz}}{\partial x^2} + \frac{(1+\nu)}{2}\frac{\partial^2\gamma_{yz}}{\partial x\partial y}\right] \quad (39)$$

$$\gamma_{yz} = \frac{h^2}{5(1-\nu)}\left[\frac{\partial^3 w}{\partial y^3} + \frac{\partial^3 w}{\partial y\partial x^2} + \frac{\partial^2\gamma_{yz}}{\partial y^2} + \frac{(1-\nu)}{2}\frac{\partial^2\gamma_{yz}}{\partial y^2} + \frac{(1+\nu)}{2}\frac{\partial^2\gamma_{xz}}{\partial x\partial y}\right] \quad (40)$$

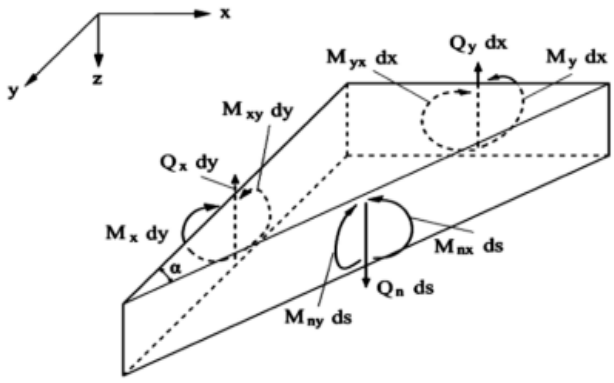

Fig. 1. Definition of the stress resultant components acting on an infinitesimal rectangular plate element and its boundary [13].

By looking at the mathematical relations of the shear angle γ_{xz} and γ_{yz}, the Bergan-Wang approach concluded that the third derivatives of the plate deflection are larger than the second derivatives of the shear strain γ_{xz} and γ_{yz}. Usually, shear deformations are controlled by a constant term for a small region of the plate, or somewhat by a linear term [23]. Therefore, the second derivatives of the shear angles are zero

or tend to zero in (39) and (40). Therefore, these expressions can be written as:

$$\gamma_{xz} = \frac{-h^2}{5(1-\nu)}\left[\frac{\partial^3 w}{\partial x^3} + \frac{\partial^3 w}{\partial x \partial y^2}\right] \quad (41)$$

$$\gamma_{yz} = \frac{-h^2}{5(1-\nu)}\left[\frac{\partial^3 w}{\partial y^3} + \frac{\partial^3 w}{\partial y \partial x^2}\right] \quad (42)$$

Now, the rotations of the normal axis on the middle plane of the plate after the deformation φ_x^R and φ_y^R can be written as a function of one variable, which is the plate deflection *w*, by substituting the new mathematical expressions of shear strain, as shown in (41) and (42), into (37) and (38), resulting in:

$$\varphi_x^R = \frac{\partial w}{\partial x} + \left[\frac{h^2}{5(1-\nu)}\left(\frac{\partial^3 w}{\partial x^3} + \frac{\partial^3 w}{\partial x \partial y^2}\right)\right] \quad (43)$$

$$\varphi_y^R = \frac{\partial w}{\partial y} + \left[\frac{h^2}{5(1-\nu)}\left(\frac{\partial^3 w}{\partial y^3} + \frac{\partial^3 w}{\partial y \partial x^2}\right)\right] \quad (44)$$

The significance of this assumption lies in its role as an approximation of the integral representing strain energy [23], due to which the Bergan-Wang formulation transforms the classical R-M plate model, originally involving transverse displacement and two rotation variables, into a single governing equation expressed solely in terms of transverse deflection *w(x,y)*. This formulation reduces the system to a sixth-order PDE, while introducing additional simplifying assumptions to minimize the number of variables [23-27]. This leads to a sixth-order PDE formulated solely in terms of *w(x,y,):*

$$q(x,y) = \frac{Eh^3}{12(1-\nu^2)}\left(\frac{\partial^4 w}{\partial x^4} + 2\frac{\partial^4 w}{\partial x^2 \partial y^2} + \frac{\partial^4 w}{\partial y^4}\right) + \frac{Eh^5}{60(1-\nu)^2(1+\nu)}\left(\frac{\partial^6 w}{\partial x^6} + 3\frac{\partial^6 w}{\partial x^2 \partial y^4} + 3\frac{\partial^6 w}{\partial x^4 \partial y^2} + \frac{\partial^6 w}{\partial y^6}\right) \quad (45)$$

This equation can be written in the compact form as:

$$q(x,y) = D_\omega \Delta\Delta w(x,y) + D_\gamma \Delta\Delta\Delta w(x,y) \quad (46)$$

where the flexural and shearing rigidities are given by:

$$D_\omega = \frac{Eh^3}{12(1-\nu^2)}$$

$$D_\gamma = \frac{Eh^5}{60(1-\nu)^2(1+\nu)}$$

This study presents examples of numerical solutions to further test the proposed numerical technique.

Because of the previous equations governing the bending of thin and moderately thick plates, it became necessary to satisfy three boundary conditions along the plate edges:

1) Clamped, Built–in, or Fixed Edge

At a fixed edge, the lateral deflection and the rotation (slope) are zero, and geometrical fixed boundary conditions can be provided [28]:

$$w = 0 \,\&\, M_{ns} = 0 \,\&\, \varphi_n = 0 \quad (47)$$

2) Free Edge

At the unloaded plate edge, the static boundary conditions can be specified for this case, as all the stresses resulting from the bending moment M_n , twisting moment M_{ns}, and shear force *Qn*, along this edge must be zero [29]. The free edge boundary conditions can be written as:

$$M_n = 0 \,\&\, M_{ns} = 0 \,\&\, Q_n = 0 \quad (48)$$

3) Simply Supported Edge

For the case of a simply supported edge, a mix of geometrical and statically boundary conditions can be provided, similarly to the clamped edge case [28]:

$$w = 0 \,\&\, M_{ns} = 0 \,\&\, M_n = 0 \quad (49)$$

This study solved the polyharmonic equation (36), which describes the deflection on a square plate subjected to a uniform distributed load with different boundary conditions, including simply supported, clamped, or free edges, as an application of the propsed method.

IV. NUMERICAL REALIZATION OF DECOUPLING AND COUPLING METHODS

In order to analyze the behavior and test the performance of the new decoupling and coupling methods, a MATLAB code was written to solve the problem of the static bending of plates, according to (36).

The numerical results are compared with those computed using the FEM and based on the R-M plate theory, for a plate with a thickness-to-span ratio (*h/a*) of 0.1 and for different cases of boundary conditions. The plate's material parameters include a Young's modulus (*E*) of 10.92 GPa and a Poisson's ratio (*v*) of 0.3. This may vary depending on the boundary conditions. The computations are done using a laptop computer with an Intel(R) Core (TM) i7-5500U CPU.

A. Case 1: Simply Supported (SSSS) Square Plate

The first example is carried out for a square plate simply supported at the four edges and subjected to a uniform load. According to the R-M plate theories, the boundary conditions in the SSSS case are:

$$\left(w = \frac{\partial^2 w}{\partial n^2} = \frac{\partial^4 w}{\partial n^4}\right)_\Gamma = 0$$

The convergence results of the plate's central deflection obtained by this method, with the exact solution are presented in Table I. For the uniform load case, a comparison between $o(h^2)$ and $o(h^4)$ in deflection *w* of the square plate at midpoint is illustrated graphically in Figure 3.

The results of the plate's central deflection obtained by the coupling and decoupling techniques with different mesh numbers, with accuracy $o(h^2)$ and compact $o(h^2)$, are compared with those obtained by the R-M plate theory in Table II.

For example, in the case of a uniform load and step=1/105, the profile of SSSS plate's displacement field on the deformed mesh is represented in Figure 2.

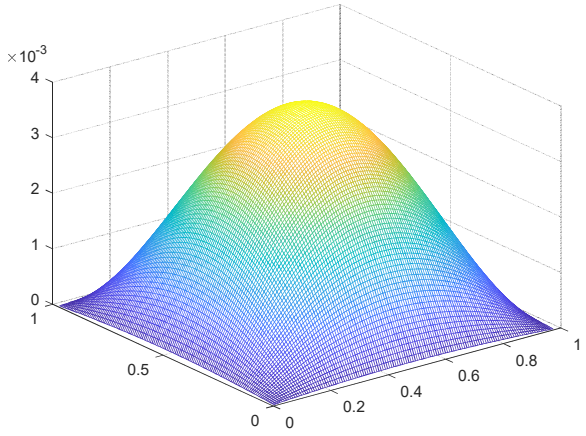

Fig. 2. Deflection profile for SSSS plate's displacement field on deformed mesh subjected to uniform load at step=1/105.

TABLE I. THE CENTRAL DEFLECTION BY IMPOSING THREE BOUNDARY CONDITIONS ($w = w_{2n} = w_{4n} = 0$) AND ABSOLUTE ERROR

Step	Rate of convergence		Maximum absolute error	
	$o(h^2)$	Compact $o(h^4)$	$E(N)$ $o(h^2)$	$E(N)$ $o(h^4)$
1/15	0.2390	0.2010	2.22E-03	4.6E-03
1/25	0.3099	0.2968	1.52E-03	1.7E-03
1/35	0.3436	0.3687	1.18E-03	9.3E-04
1/45	0.3639	0.3963	9.77E-04	6.5E-04
1/55	0.3785	0.4180	7.31E-04	4.4E-04
1/65	0.3910	0.4342	5.18E-04	2.7E-04
1/75	0.4058	0.4466	3.58E-04	1.5E-04
1/85	0.4417	0.4566	1.99E-04	5E-05
1/95	0.4494	0.46139	1.22E-04	2.1E-06
1/105	0.4571	0.4614	4.5E-05	1.1E-06

TABLE II. COMPARISON OF CENTRAL DEFLECTION w FOR SSSS CASE

h/a	**0.1**
Uniform load	
R-M theory [30]	0.4616
BWRE36 (16x16) [13]	0.4471
BWRE36 (32x32) [13]	0.4703
Decoupling technique $o(h^2)$	0.4571
Compact $o(h^4)$	0.4614

The convergence analysis, depicted in Figure 3, demonstrates how the conversion rates vary with a decreasing grid size h. Using the R-M method as a reference, the relative error analysis reveals significant improvements in accuracy with the proposed method. The $o(h^4)$ variant shows remarkably lower mean relative errors of 9.58%, compared to other methods, with BWRE 24, BWRE 36, and $o(h^2)$ exhibiting substantially higher mean errors of 56.71%, 53.93%, and 48.89%, respectively.

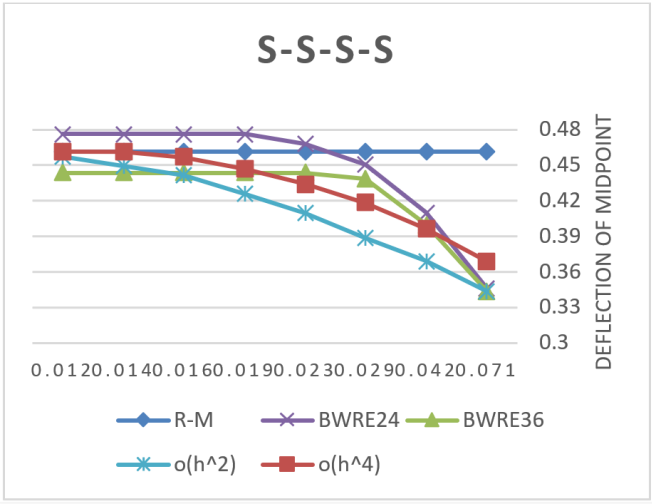

Fig. 3. Comparison of deflection w at the midpoint of an SSSS square plate using $o(h^2)$ and $o(h^4)$ schemes at various step sizes.

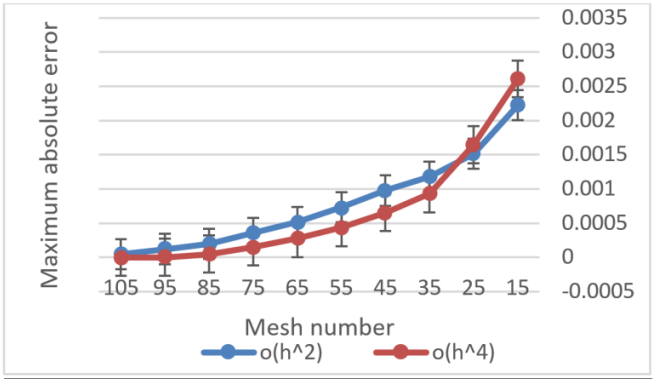

Fig. 4. Absolute error with various mesh sizes for different levels of accuracy for case 1.

B. Case 2: SCSC Square Plate

In this example, two opposite edges are simply supported and the other two edges are clamped with a deflection profile, as portrayed in Figure 5. These two boundary conditions are represented as:

$$\left(w = \frac{\partial^2 W}{\partial y^2} = \frac{\partial^4 W}{\partial y^4}\right)_{\substack{y=0 \\ y=b}} = 0$$

$$\left(w = \frac{\partial w}{\partial x} = \frac{\partial^3 W}{\partial x^3}\right)_{\substack{x=0 \\ x=a}} = 0$$

The results of the plate's central deflection obtained by decoupling and coupling with different mesh numbers, with accuracy $o(h^2)$ and compact $o(h^4)$ are compared in Table III, and this comparison is represented graphically in Figure 6.

Table IV presents a comparison between the results from this method and those obtained by the R-M plate theory.

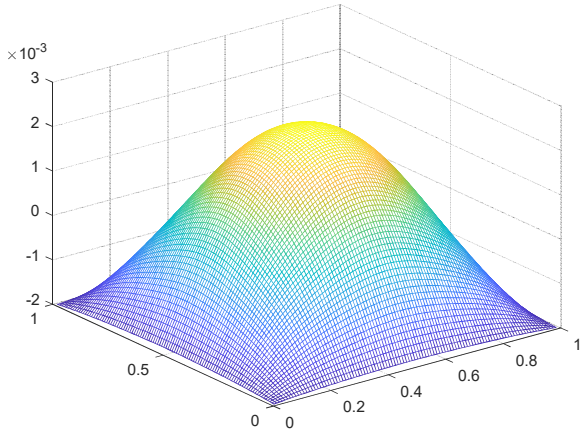

Fig. 5. Deflection profile for SCSC plate's displacement field on deformed mesh subjected to uniform load at step = 1/105.

TABLE III. THE CENTRAL DEFLECTION BY IMPOSING THREE BOUNDARY CONDITIONS FOR SIMPLY SUPPORTED EDGES ($w = w_{2n} = w_{4n} = 0$) AND CLAMPED EDGES ($w = w_n = w_{3n} = 0$).

Step	Rate of convergence		Maximum absolute error	
	$o(h^2)$	Compact $o(h^4)$	$E(N)$ $o(h^2)$	$E(N)$ $o(h^4)$
1/15	0.00195	0.002008	2.6E-04	2.02E-04
1/25	0.002008	0.00211	2.02E-04	9.96E-05
1/35	0.0020655	0.002156	1.45E-04	5.42E-05
1/45	0.002094	0.00218	1.16E-04	2.98E-05
1/55	0.002113	0.002195	9.7E-05	1.46E-05
1/65	0.002152	0.002202	5.8E-05	9E-06
1/75	0.002181	0.002203	2.9E-05	8.34E-06
1/85	0.002188	0.002206	2.2E-05	4.29E-06
1/95	0.002204	0.002213	6E-06	5.82E-07
1/105	0.00221	0.002214	1.9E-07	3.86E-07

TABLE IV. COMPARISON OF CENTRAL DEFLECTION w RESULTS FOR THE SCSC CASE.

h/a	0.1
Uniform load	
R-M theory [31]	0.2200
BWRE36 (16×16) [32]	0.2240
BWRE36 (32×32) [32]	0.2327
Decoupling method $o(h^2)$	0.2210
Compact $o(h^4)$	0.2214

As seen in Figure 6, as the grid size h decreased, all methods demonstrated improved conversion rates, with the proposed decoupling method at $o(h^4)$ consistently yielding the most accurate results. The convergence plot illustrates that the $o(h^4)$ method closely tracks the reference values across all grid sizes, while the R-M and BWRE 36 methods exhibit larger deviations, particularly at finer resolutions.

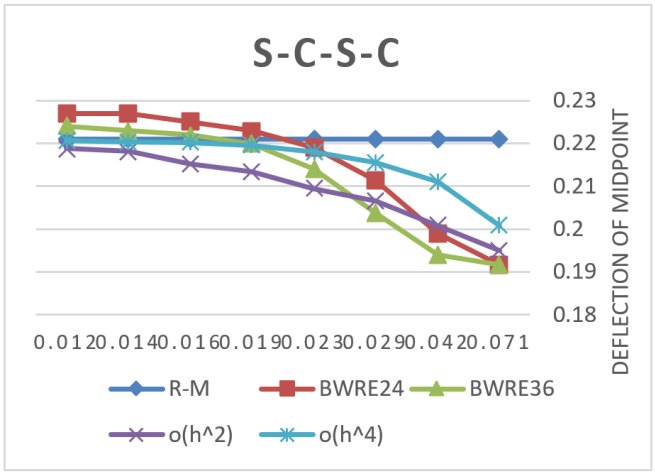

Fig. 6. Comparison of deflection w at the midpoint of an SCSC square plate using $o(h^2)$ and $o(h^4)$ schemes at various step sizes.

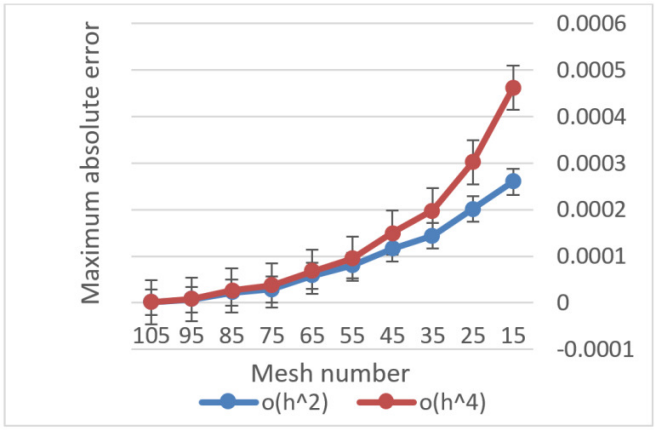

Fig. 7. Absolute error with various mesh sizes for different levels of accuracy for case 2.

To quantify these differences, a relative error analysis reveals that the mean relative errors for the BWRE 24 and BWRE 36 methods are significantly higher than those for the $o(h^2)$ and $o(h^4)$ methods. Specifically, the mean relative errors were 6.80% for BWRE, 24, 5.11% for BWRE 36, 3.97% for $o(h^2)$, and 3.17% for $o(h^4)$. The maximum relative errors further highlight the superiority of the proposed method, with BWRE 24 and BWRE 36 reaching up to 8.22% and 8.60%, respectively, compared to 4.87% for $o(h^4)$ and 5.71% for $o(h^2)$.

C. Case 3: Cantilever (CFFF) Square Plate

The third example is a square plate clamped at one edge and free at the other edges, subjected to a uniform load at the plate. The normalized deflection at the midpoint of the free side $y = a$ of a CFFF square plate is computed for the thickness/length ratios of the plate (h/a = 0.1) and is subjected to uniform load, as shown in Figure 8, by imposing boundary conditions:

$$W|_{y=0} = \frac{\partial W}{\partial y}\Big|_{y=0} = 0$$

$$\left(\frac{\partial^2 W}{\partial y^2}+\frac{\partial^2 W}{\partial x^2}\right)_{y=b}=0$$

$$\left(\frac{\partial^3 W}{\partial y^3}+\frac{\partial^3 W}{\partial x^2 \partial y}\right)_{y=b}=0$$

$$\left(\frac{\partial^2 W}{\partial x^2}+\frac{\partial^2 W}{\partial y^2}\right)_{\substack{x=0\\x=a}}=0$$

$$\left(\frac{\partial^3 W}{\partial x^3}+\frac{\partial^3 W}{\partial x \partial y^2}\right)_{\substack{x=0\\x=a}}=0$$

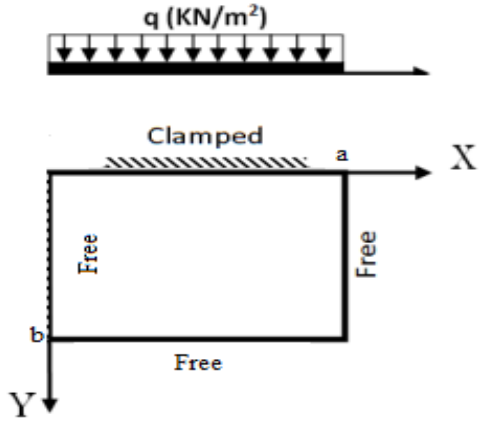

Fig. 8. CFFF plate subjected to uniform load.

The results of the plate's central deflection obtained using both decoupling and coupling techniques, based on the R-M plate theory under its standard boundary conditions and two additional boundary conditions (case1: $w_{2n}=0$, case2: $w_{2n}=w_{3n}=0$), are compared with those derived directly from the R-M theory, as displayed in Table VI. The deflection shapes obtained are consistent with those reported in [13, 32], where similar CFFF plate configurations under uniform loading were analyzed. The profile of the CFFF plate's displacement field on the deformed mesh is represented in Figure 9.

Using the Bergan-Wang model as the reference, the error analysis demonstrates the superior accuracy of the proposed methods. The $o(h^4)$ variant demonstrates excellent accuracy with a mean relative error of only 2.30%, while the $o(h^2)$ variant shows a slightly higher, but still impressive mean error of 3.45%. BWRE 24 exhibits a notably higher mean error of 7.74%, while BWRE 36 performs better with a mean error of 1.33%.

The maximum relative errors further validate the robustness of the proposed methods, with $o(h^4)$ reaching only 3.78% deviation and $o(h^2)$ 6.01%. BWRE 24 demonstrates the highest maximum error at 25.25%, while BWRE 36 maintains better stability with a maximum error of 4.18%.

These results demonstrate that the proposed decoupling method at $o(h^4)$ not only achieves higher accuracy, but also exhibits a more robust convergence behavior compared to other approaches. This makes it a superior choice for applications requiring precise and reliable conversion rates.

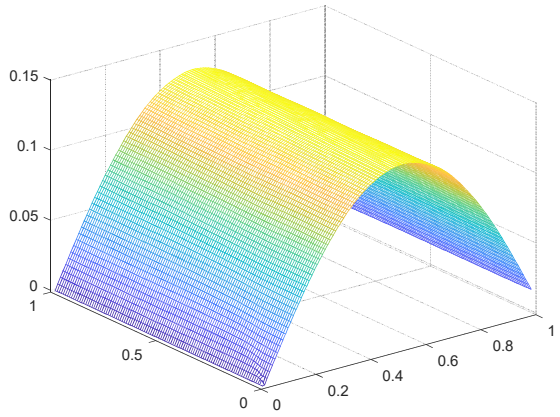

Fig. 9. Deflection profile for CFFF plate's displacement field on deformed mesh subjected to uniform load at step = 1/105.

TABLE V. CONVERSION RATE OF DEFLECTION FOR CFFF CASE UNDER UNIFORM LOAD AND CORRESPONDING ABSOLUTE ERROR

Step	Rate of convergence		Maximum absolute error	
	$o(h^2)$	Compact $o(h^4)$	$E(N)$ $o(h^2)$	$E(N)$ $o(h^4)$
1/15	0.09969	0.11235	0.031809505	0.01915
1/25	0.116849	0.121365	0.014650501	0.01013476
1/35	0.1236	0.126524	7.9E-03	4.976E-03
1/45	0.126705	0.128421	4.7949E-03	3.29E-03
1/55	0.128109	0.129082	3.3915E-03	2.479E-03
1/65	0.129426	0.129895	2.074E-03	1.605E-03
1/75	0.129924	0.130121	1.5761E-03	1.3795E-03
1/85	0.130132	0.13091	1.3682E-03	1.3087E-03
1/95	0.130629	0.13107	8.714E-04	4.8477E-04
1/105	0.131006	0.13114	4.9374E-04	3.57E-04

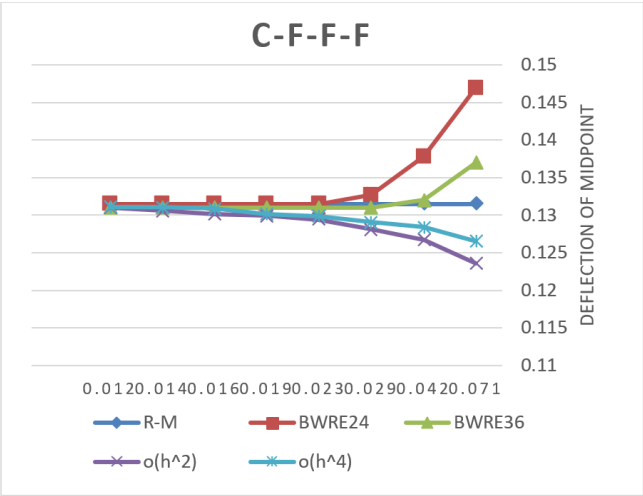

Fig. 10. Comparison of deflection w at the midpoint of an CFFF square plate using $o(h^2)$ and $o(h^4)$ schemes at various step sizes.

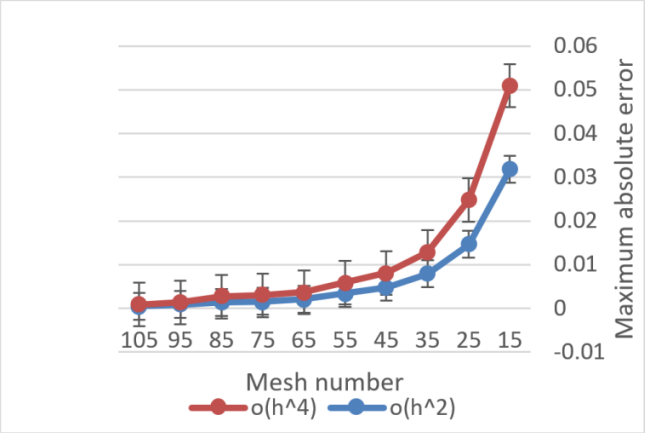

Fig. 11. Absolute error with various mesh sizes for different levels of accuracy.

TABLE VI. COMPARISON OF CENTRAL DEFLECTION *W* RESULTS FOR CFFF

Uniform load	
R-M theory [32]	0.1315
BWRE24 (32 × 32) [13]	0.1312
BWRE36 (16 × 16) [13]	0.1309
Decoupling and coupling techniques	
Case 1: $w_{2n} = 0$	0.13609
Case 3: $w_{2n} = w_{3n} = w_{4n} = 0$	0.13410
Case 2: $w_{2n} = w_{3n} = 0$	0.131006 $o(h^2)$ 0.1311 Compact $o(h^4)$

V. CONCLUSION

This paper provides a novel representation of the Reissner-Mindlin (R-M) theory by modeling plate bending with a single sixth-order equation and straightforward geometric boundary conditions. In contrast to conventional schemes, it uses a high-order Compact Finite Difference (CFD) discretization, greatly improving the numerical accuracy and convergence behavior. A thorough numerical validation of the framework is conducted against contemporary benchmark approaches, such as Finite Element Methods (FEMs). Quantitative comparisons are made regarding the convergence rates, stress distribution, and displacement accuracy. The accompanying MATLAB implementation underscores the method's simplicity and adaptability to various bending scenarios. The results obtained from the new finite difference formulation show a closer agreement with the R-M theory, which traditionally uses a system of three coupled second-order Partial Differential Equations (PDEs) to model deflection. Finally, by leveraging the Laplace operator and its higher-order forms, the proposed decoupling strategy avoids the need for complex polyharmonic operator stencils, thereby streamlining the computational process.

Furthermore, the proposed methodology lays the groundwork for future investigations involving complex engineering applications, including non-standard boundary conditions, variable material properties, handling irregular geometries and non-uniform meshes, and non-linear deformation analyses. However, generalizing the CFD method to complex geometries is nontrivial and remains an open research area. As part of future work, hybrid discretization approaches, such as coordinate transformations, embedded grids, or coupling with meshless methods, will be explored to systematically address this limitation.

CONFLICT OF INTEREST

The authors declare that they have no known conflicts of interest that could have appeared to influence the work reported in this paper.

DATA AVAILABILITY

The datasets generated and/or analyzed during the current study are available from the corresponding author upon reasonable request.

REFERENCES

[1] M. Mierzwiczak and J. A. Kołodziej, "Comparison of three meshless methods for 2D harmonic and biharmonic problems," *Engineering Analysis with Boundary Elements*, vol. 118, pp. 157–168, Sep. 2020, https://doi.org/10.1016/j.enganabound.2020.04.003.

[2] B. N. Mishra and R. K. Mohanty, "Single cell Numerov type discretization for 2D biharmonic and triharmonic equations on unequal mesh," *Journal of Mathematical and Computational Science*, vol. 3, no. 1, pp. 242–253, 2013.

[3] M. Dehghan and A. Mohebbi, "Solution of the two dimensional second biharmonic equation with high-order accuracy," *Kybernetes*, vol. 37, no. 8, pp. 1165–1179, Sep. 2008, https://doi.org/10.1108/03684920810884964.

[4] R. K. Mohanty, S. Karaa, and U. Arora, "Fourth order nine-point unequal mesh discretization for the solution of 2D nonlinear elliptic partial differential equations," *Neural, Parallel and Scientific Computations*, vol. 14, no. 4, pp. 453–470, Dec. 2006.

[5] C. Liebold, B. M. Dawwas, "Numerical Solution of the Tri-harmonic Kirchhoff Plate Equation Resulting from a Strain Gradient Theory," in *Advanced Structured Materials*, Cham: Springer International Publishing, 2019, pp. 271–290.

[6] S. Wang *et al.*, "Interactive PDE patch-based surface modeling from vertex-frames," *Engineering with Computers*, vol. 38, no. 5, pp. 4367–4385, Oct. 2022, https://doi.org/10.1007/s00366-022-01602-z.

[7] H. S. El Gendy, M. S. Semary, T. M. Rageh, and K. Hassan, "An Efficient Implementation of Coupling and Decoupling Scheme for Biharmonic Equation," *The International Conference on Mathematics and Engineering Physics*, vol. 10, no. 10, pp. 1–20, May 2024, https://doi.org/10.21608/icmep.2024.390916.

[8] H. Dastour and W. Liao, "An optimal 13-point finite difference scheme for a 2D Helmholtz equation with a perfectly matched layer boundary condition," *Numerical Algorithms*, vol. 86, no. 3, pp. 1109–1141, Mar. 2021, https://doi.org/10.1007/s11075-020-00926-5.

[9] I. Altas, J. Erhel, and M. M. Gupta, "High Accuracy Solution of Three-Dimensional Biharmonic Equations," *Numerical Algorithms*, vol. 29, no. 1–3, pp. 1–19, Mar. 2002, https://doi.org/10.1023/a:1014866618680.

[10] M. Ben-Artzi, J.-P. Croisille, and D. Fishelov, "A Fast Direct Solver for the Biharmonic Problem in a Rectangular Grid," *SIAM Journal on Scientific Computing*, vol. 31, no. 1, pp. 303–333, Jan. 2008, https://doi.org/10.1137/070694168.

[11] D. Quang A and M. Xuan Thao, "Iterative method for solving a problem with mixed boundary conditions for biharmonic equation arising in fracture mechanics," *Boletim da Sociedade Paranaense de Matemática*, vol. 31, no. 1, Nov. 2011, Art.no. 65, https://doi.org/10.5269/bspm.v31i1.11728.

[12] K. Hassan, "Review on Solving 2-D Poisson Problem by Finite and Compact Difference Methods."

[13] K. Hassan, E. Ali, and M. Tawfik, "Finite Elements for the One Variable Version of Mindlin-Reissner Plate," *Latin American Journal of Solids*

and Structures, vol. 17, no. 6, 2020, https://doi.org/10.1590/1679-78256170.

[14] D. Q. Long, "Numerical Solution of a Boundary Value Problem for Triharmonic Equation," *Applied Mathematical Sciences*, vol. 6, pp. 3073–3079, 2012.

[15] E. C. Romao and L. H. P. De Assis, "Numerical Simulation of 1D Unsteady Heat Conduction-Convection in Spherical and Cylindrical Coordinates by Fourth-Order FDM," *Engineering, Technology & Applied Science Research*, vol. 8, no. 1, pp. 2389–2392, Feb. 2018, https://doi.org/10.48084/etasr.1724.

[16] Z. Li and K. Pan, "High Order Compact Schemes for Flux Type BCs," *SIAM Journal on Scientific Computing*, vol. 45, no. 2, pp. A646–A674, Apr. 2023, https://doi.org/10.1137/21m1444771.

[17] H. Wang, Y. Zhang, X. Ma, J. Qiu, and Y. Liang, "An efficient implementation of fourth-order compact finite difference scheme for Poisson equation with Dirichlet boundary conditions," *Computers & Mathematics with Applications*, vol. 71, no. 9, pp. 1843–1860, May 2016, https://doi.org/10.1016/j.camwa.2016.02.022.

[18] D. N. Tien, N. X. Tung, and N. N. Lam, "Analytical Solution for Bending Steel Concrete Composite Plates considering the Shear Deformation Effect," *Engineering, Technology & Applied Science Research*, vol. 14, no. 5, pp. 16090–16094, Oct. 2024, https://doi.org/10.48084/etasr.7801.

[19] H.-T. Thai and D.-H. Choi, "Analytical solutions of refined plate theory for bending, buckling and vibration analyses of thick plates," *Applied Mathematical Modelling*, vol. 37, no. 18–19, pp. 8310–8323, Oct. 2013, https://doi.org/10.1016/j.apm.2013.03.038.

[20] E. Reissner and G. B. Thomas, "On bending of elastic plates," *Journal of Mathematical Physics*, vol. 25, pp. 55–68, 1946.

[21] R. D. Mindlin, "Influence of Rotatory Inertia and Shear on Flexural Motions of Isotropic, Elastic Plates," in *The Collected Papers of Raymond D. Mindlin Volume I*, New York, NY: Springer New York, 1989, pp. 225–232.

[22] C. M. Wang, G. T. Lim, J. N. Reddy, and K. H. Lee, "Relationships between bending solutions of Reissner and Mindlin plate theories," *Engineering Structures*, vol. 23, no. 7, pp. 838–849, Jul. 2001, https://doi.org/10.1016/s0141-0296(00)00092-4.

[23] P. G. Bergan and X. Wang, "Quadrilateral plate bending elements with shear deformations," *Computers & Structures*, vol. 19, no. 1–2, pp. 25–34, Jan. 1984, https://doi.org/10.1016/0045-7949(84)90199-8.

[24] A. M. D'Altri, L. Patruno, S. De Miranda, and E. Sacco, "First-order VEM for Reissner–Mindlin plates," *Computational Mechanics*, vol. 69, no. 1, pp. 315–333, Jan. 2022, https://doi.org/10.1007/s00466-021-02095-1.

[25] A. S. Pechstein and J. Schöberl, "The TDNNS method for Reissner–Mindlin plates," *Numerische Mathematik*, vol. 137, no. 3, pp. 713–740, Nov. 2017, https://doi.org/10.1007/s00211-017-0883-9.

[26] V. L. Salerno and M. A. Goldberg, "Effect of Shear Deformations on the Bending of Rectangular Plates," *Journal of Applied Mechanics*, vol. 27, no. 1, pp. 54–58, Mar. 1960, https://doi.org/10.1115/1.3643934.

[27] H. Abdalla and K. Hassan, "On the Bergan-Wang approach for moderately thick plates," *Communications in Applied Numerical Methods*, vol. 4, no. 1, pp. 51–58, Jan. 1988, https://doi.org/10.1002/cnm.1630040108.

[28] Y. W. Kwon and H. Bang, *The Finite Element Method Using MATLAB*, 0 ed. CRC Press, 2018.

[29] H. C. Huang, Static and Dynamic Analyses of Plates and Shells: Theory, Software and Applications. London, UK: Springer London, 1989.

[30] J. Jirousek, A. Wróblewski, and B. Szybiński, "A new 12 DOF quadrilateral element for analysis of thick and thin plates," *International Journal for Numerical Methods in Engineering*, vol. 38, no. 15, pp. 2619–2638, Aug. 1995, https://doi.org/10.1002/nme.1620381508.

[31] G. P. Bazeley, K. Cheung, B. M. Irons, and O. C. Zienkiewicz, "Triangular elements in bending conforming and nonconforming solutions," in *Proceedings of Matrix methods in structural mechanics*, Wright-Patterson AF Base, Ohio, Nov. 1966, pp. 547–576.

[32] H. Askes and A. R. Wallace, "Dynamic Bergan–Wang theory for thickplates," *Mathematics and Mechanics of Complex Systems*, vol. 10, no. 2, pp. 191–204, Oct. 2022, https://doi.org/10.2140/memocs.2022.10.191.

[33] C. Fo-van, "Bending of uniformly cantilever rectangular plates," *Applied Mathematics and Mechanics*, vol. 1, no. 3, pp. 371–383, Dec. 1980, https://doi.org/10.1007/bf01874559.